RESEARCH PAPER

Sintering mechanisms and mechanical properties of joints bonded using silver nanoparticles for electronic packaging applications

Jianfeng Yan · Guisheng Zou · Lei Liu · Dongyue Zhang · Hailin Bai · Ai-ping Wu · Y. Norman Zhou

Abstract The low-temperature bonding process using metal nanoparticles has attracted considerable attention due to its potential applications including electronic packaging. However, the fundamental understanding of this advanced bonding technology is still limited. In this study, Ag nanoparticle paste used as a bonding material is prepared by the chemical reduction method. The sintering behaviors of Ag nanoparticles during the bonding process were investigated using the classical sphere-to-sphere approach. At low sintering temperatures (160–250 °C), the calculated mechanism-characteristic exponent n is 7.9, which indicates that surface diffusion is the dominant diffusion mechanism. With the increase of temperatures (300–350 °C), mechanism-characteristic exponent n changes to 3.75. This indicates that volume diffusion is probably the prevailing diffusion mechanism at this stage. Based on the classical sphere-to-sphere model, the relationship between the joint strength evolution and neck growth of Ag particles is revealed. It is found that the joint strength is proportional to square of neck size ratio $(x/r)^2$ of sintered Ag particles.

J. Yan (✉) · G. Zou · L. Liu · D. Zhang · H. Bai · A.-p. Wu · Y. N. Zhou
Department of Mechanical Engineering, Tsinghua University, Beijing 100084, China
e-mail: yanjf@tsinghua.org.cn

J. Yan
National Engineering and Technological Research Center for Nonferrous Metal Composites, General Research Institute for Nonferrous Metals, Beijing 100088, China

Y. N. Zhou
Centre of Advanced Materials for Joining, Department of Mechanical and Mechatronics Engineering, University of Waterloo, 200 University Avenue West, Waterloo, ON N2L 3G1, Canada

1 Introduction

Metal nanoparticles (NPs) are of great interest due to their potential applications in such fields as catalysis, biology, electronics, optoelectronics, and information technology [1–6]. When particles are reduced in size to nanoscale, their characteristics are different from those of the bulk state [7]. Especially, the increase of diffusion coefficient and decrease of melting point are obvious compared with those for the bulk state [8–12]. Due to the size effect, metal nanoparticles show bright prospects in the electronics industry, such as flat panel displays, organic electronics, and low-cost disposable microelectronic devices on plastic substrates [13–19]. For example, low-temperature interconnection processes using metallic nanoparticle pastes, including silver [16–22], copper [23], and gold [24], appear to be a promising alternative for lead-free electronic packaging and flexible electronic interconnections. Furthermore, the good expected performance at high-temperature environments is another unique property of metal nanoparticles as a bonding material. Metal nanoparticles show lower sintering temperature, due to high specific surface activity. During the sintering process, the nanoscale structure changes to microscale or bulk structures. Thus, this bonding technology allows a lower temperature process but can service at higher-temperature environment. The bonding materials can be used in the devices that applied at high-temperature environment and wide band gap semiconductor devices [18, 25, 26].

Metal nanoparticles have attracted considerable interest as interconnect materials fueled by its potential application in electronic packaging technology. In most of these manufacturing operations of metal nanoparticles for devices, the sintering of nanoparticles is necessary [4–6, 16–19, 23–26]. However, the fundamental understanding of the sintering mechanisms and mechanical properties of joints using nanoparticles is still limited [16–19, 23–26]. In this paper, we investigated the sintering bonding process using Ag nanoparticles based on the classical sphere-to-sphere model. The sintering mechanisms of Ag nanoparticles during the sintering bonding process and the mechanical properties of joints related to the microstructure are discussed based on the sintering model.

2 Experimental details

Polyvinylpyrrolidone (PVP K-30), silver nitrate ($AgNO_3$), ethylene glycol (EG), acetone, and ethanol were all analytical grade and used without further purification.

Ag nanoparticle paste was prepared by the chemical reduction method [19, 22]. Firstly, silver nanoparticle solution was synthesized based on the modified polyol method [2]. The $AgNO_3$ was reduced in EG solution, and polyvinylpyrrolidone (PVP) was used as a protecting agent to prevent it from aggregation. The polyol in the polyol process acts as both a solvent and a reducing agent. The reduction mechanism of Ag nanoparticles by EG probably involves the following chemical reactions [27]:

$$2HOCH_2-CH_2OH = 2CH_3CHO + 2H_2O \qquad (1)$$

$$2CH_3CHO + 2AgNO_3 = CH_3CO-COCH_3 + 2Ag \\ + 2HNO_3 \qquad (2)$$
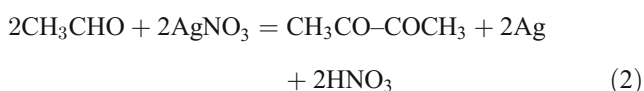
Ag nanoparticle paste was prepared by condensing Ag nanoparticle solution with a centrifuge at 7000 rpm for 20 min without further addition of organic component.

Both the sintering and bonding experiments using Ag nanoparticle paste were conducted in air atmosphere. The bonding specimens were Ni/Ag-coated Cu discs as shown in Fig. 1. The nickel plating (2 μm) and then silver plating (4 μm) were applied by electrolysis to protect the Cu discs from oxidation. Ag nanoparticle paste was coated on the surfaces of the two Ag-plated Cu discs. The specimens were dried at 80 °C to remove the low boiling point component in the paste. The sintering process was performed in an oven at different sintering temperatures. During the bonding process, the smaller specimen (with diameter of 6 mm) was placed on
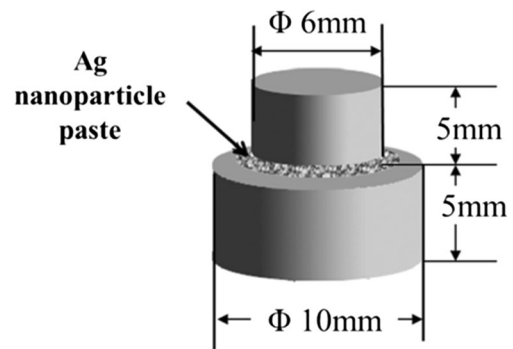
Fig. 1 Schematic illustration of the bonding specimens of big cylinder (Φ=10 mm, h=5 mm) and small cylinder (Φ=6 mm, h=5 mm)

top of the bigger specimen (with diameter of 10 mm) after enough Ag nanoparticle paste had been gathered. The bonding of Ag-plated Cu discs was conducted at a temperature range of 160–350 °C with an assistant pressure of 5 MPa.

The size diameters and morphologies of the Ag nanoparticles were analyzed using scanning electron microscopy (SEM) and transmission electron microscopy (TEM). The batch of neck size and particle size was measured for both fractured necks and particles on contact by SEM. The crystal structure of the Ag nanoparticle paste was obtained by X-ray diffractometry (XRD). The organic residues in Ag nanoparticle paste after sintering were detected by Fourier transform infrared spectroscopy (FTIR). The strength of the joint was measured as shear strength measured using a Gleeble 1500D thermomechanical simulator with a displacement speed of 5 mm min^{-1} at room temperature.

3 Results and discussion

3.1 Characteristics of Ag nanoparticles

Figure 2 displays the SEM and TEM images of Ag nanoparticles synthesized by a typical method. It can be seen that these Ag nanoparticles are mainly spherical in shape, with a mean diameter of about 40 nm. TEM image of the synthesized Ag nanoparticles shows that a thin layer of organic shell was coated on the surface of particles, which can prevent them from coalescence. The XRD diffraction pattern recorded from the Ag nanoparticle paste displays the peak characteristics of metallic silver. The reflection peaks are indexed as the fcc (111), (200), (220), and (311) planes, which indicates that these Ag nanoparticles are well crystallized.

3.2 Sintering mechanisms of the Ag nanoparticles

After sintering at 250 °C for 30 min in air, two adjacent sphere Ag particles are sintered together and the interparticle neck is formed between the particles, as shown in Fig. 3. It is thought

Fig. 2 SEM (**a**) and TEM (**b**) images of Ag nanoparticles (*inset* showing the XRD patterns of Ag nanoparticles)
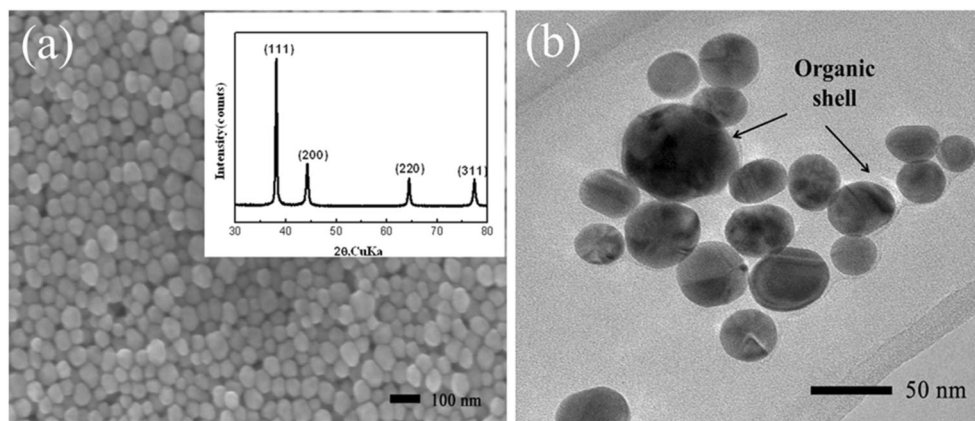

that the sintering of Ag nanoparticles is crucial for the joint formation, since the joint is usually fractured in the sintered Ag layer [16, 17, 22]. According to the sintering theory, sintering process can be divided into three stages referred to as the initial stage, the intermediate stage, and the final stage. The initial stage of sintering generally consisted of fairly rapid interparticle neck growth by different material transports to a certain extent [28]. The initial stage of sintering, as indicated by Coble, involves no grain growth [29]. According to work of Rahaman, the initial stage sintering occurs until the radius of the neck between the particles has reached a value of ~0.4–0.5 of the particle radius [30].

Different sintering models have been developed to describe the sintering [31–33]. We base our analysis on the classical

sphere-to-sphere model which was first described by Frenkel [31]. The sphere-to-sphere model for the initial stage consists of two equal-sized spheres in contact as shown in Fig. 3d. The neck formed between two particles (with diameter D and radius r) is assumed to be circular (with diameter X and radius x).

Based on the sintering theory, different types of material transport may correspond to neck growth during the sintering process. These transports might consist of viscous flow, volume diffusion, grain boundary diffusion, and surface diffusion. Theoretical equations reported for different sintering mechanisms are summarized in Table 1 [31, 33, 34]. These results indicate that the different neck growth equations are related to different types of material transport during the

Fig. 3 TEM images (**a**, **b**) and SEM image (**c**) showing the neck formed between the two adjacent Ag particles after sintering at 250 °C for 30 min in air. **d** A schematic based on sphere-to-sphere model explaining the sintering of Ag nanoparticles. r and D are the radius and diameter of the particle, respectively; x and X are the radius and diameter of the neck circular, respectively. *Arrows* indicate the important atomic diffusion paths between two contacting particles
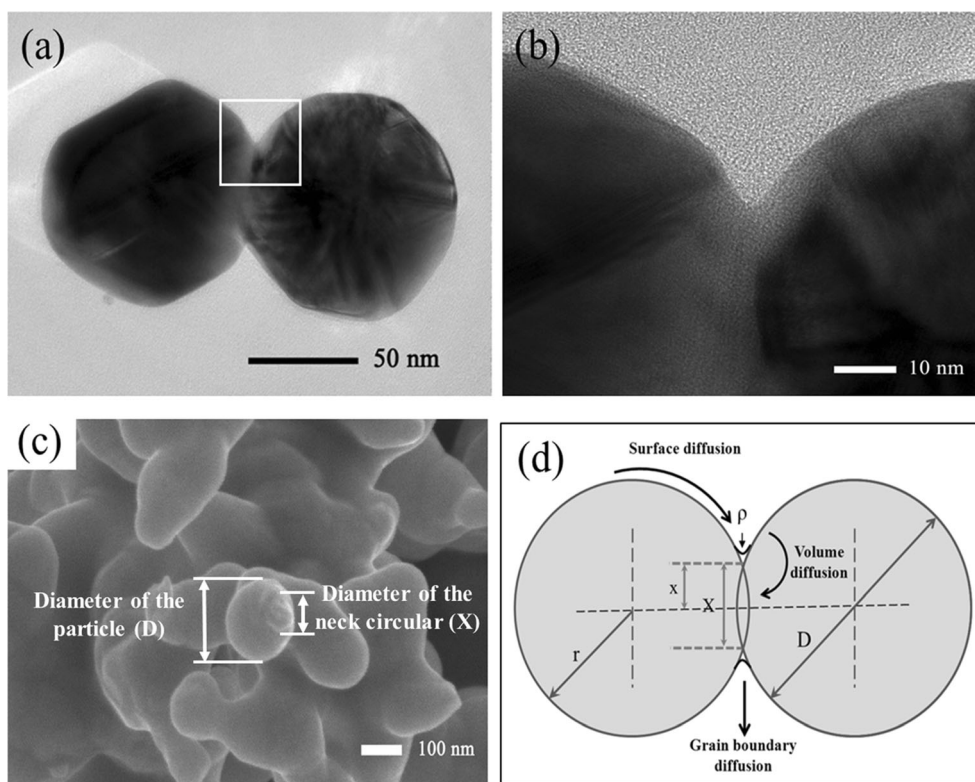
Table 1 Theoretical equations for different types of material transport during neck growth

Material transport types	Author	Theoretical equation for neck growth	$(x/r)^n = Bt$	Exponent n
Viscous flow	Frenkel [29]	$\dfrac{x^2}{r} = \dfrac{3\gamma}{2\eta(T)}t$	$\left(\dfrac{x}{r}\right)^2 = \dfrac{3\gamma}{2\eta(T)r}t$	2
Volume diffusion	Rockland [32]	$\dfrac{x^4}{r} = \left(\dfrac{16\sigma\delta^3}{kT}\right)D_v t$	$\left(\dfrac{x}{r}\right)^4 = \left(\dfrac{16\sigma\delta^3}{kTr^3}\right)D_v t$	4
	Kuczynski [31]	$\dfrac{x^5}{r^2} = \left(\dfrac{40\sigma\delta^3}{kT}\right)D_v t$	$\left(\dfrac{x}{r}\right)^5 = \left(\dfrac{40\sigma\delta^3}{kTr^3}\right)D_v t$	5
Grain boundary diffusion	Rockland [32]	$\dfrac{x^6}{r^2} = \left(\dfrac{48\sigma\delta^4}{\pi kT}\right)D_b t$	$\left(\dfrac{x}{r}\right)^6 = \left(\dfrac{48\sigma\delta^4}{\pi kTr^4}\right)D_b t$	6
Surface diffusion	Kuczynski [31]	$\dfrac{x^7}{r^3} = \left(\dfrac{56\sigma\delta^4}{kT}\right)D_s t$	$\left(\dfrac{x}{r}\right)^7 = \left(\dfrac{56\sigma\delta^4}{kTr^4}\right)D_s t$	7

γ is the surface energy of the material which is almost independent on the temperature; $\eta(T)$ is the temperature dependence shear viscosity; r is the initial particle radius; x is the radius of the interface, assumed to be circular; t is the time; σ is the surface tension of material; δ is the interatomic distance; k is the Boltzmann constant; T is the absolute temperature; D_v, D_b, and D_s are the coefficients of volume self-diffusion, grain boundary self-diffusion, surface diffusion coefficient, respectively; and n is a mechanism-characteristic exponent

sintering process. In the initial stage of sintering, the particle radius is assumed to be unchanged. As shown in Table 1, the sintering equations for different sintering mechanisms can be generally expressed as follows [33]:

$$(x/r)^n = Bt \qquad (3)$$

where x/r is the ratio of the interparticle neck radius to the particle radius. B is a constant (which includes particle size, temperature, and geometric and material terms). t is the sintering time and n is a mechanism-characteristic exponent that is depended on the mass transport process (viscous flow: $n=2$; volume diffusion: $n=4$–5; grain boundary diffusion: $n=6$; surface diffusion: $n=7$).

Since exponent n is dependent on the sintering mechanism, the measurement of n may provide information on the dominant sintering mechanisms. The value of n can be calculated based on the following equation:

$$\log(x/r) = (1/n)\log(t) + (1/n)\log(B) \qquad (4)$$

In order to elucidate the dominant sintering mechanism of Ag nanoparticles, the relationship between neck diameter and time is established. Figure 4 shows experimental logarithm plots of these curves of the evolution of the interparticle neck size ratio (x/r) with sintering time. An approximate linear relation is existed between the $\log(x/r)$ and $\log(t)$. The values of inverse slope at the sintering temperatures of 160, 200, and 250 °C are 6.7, 8.8, and 8.4, respectively (the mean value is 7.9). This result indicates that surface diffusion may be the dominant diffusion mechanism at sintering temperature range of 160–250 °C. The surface diffusion at lower sintering temperature may be related with the high specific surface activity of Ag nanoparticles at this stage. When the sintering temperatures increase to 300–350 °C, the inverse slope changes to 3.7 and 3.8 (the mean value is 3.75). This indicates that

volume diffusion is probably the prevailing diffusion mechanism at sintering temperature range of 300–350 °C.

FTIR analysis was performed to reveal the changes of organic residues in Ag nanoparticle paste during the sintering. Figure 5 presents the FTIR spectrum of polyvinylpyrrolidone (PVP) and Ag nanoparticle paste after being sintered at temperatures of 160–350 °C. Characteristic bands of PVP are found at 2953 cm^{-1} (C–H stretch) and 1677 cm^{-1} (C=O stretch). For the spectrum of Ag nanoparticle paste after being sintered at 160 °C, the peaks of C=O are red shift to 1633 cm^{-1}. The changes of the spectrum indicate that an interaction exists between the carboxyl oxygen atom (C=O bonding) of PVP and the Ag nanoparticle surface [35]. It is worth mentioning that the spectrum at 2893 cm^{-1} (C–H stretch) disappears and the spectrum at 1032 cm^{-1} (C–N stretch) is weakened greatly for the Ag nanoparticle paste after being sintered at 300 and 350 °C. This indicates that the PVP is probably destroyed at this temperature. It seems that the PVP coated on the Ag particles plays an important role to affect the sintering mechanisms. As the sintering temperature
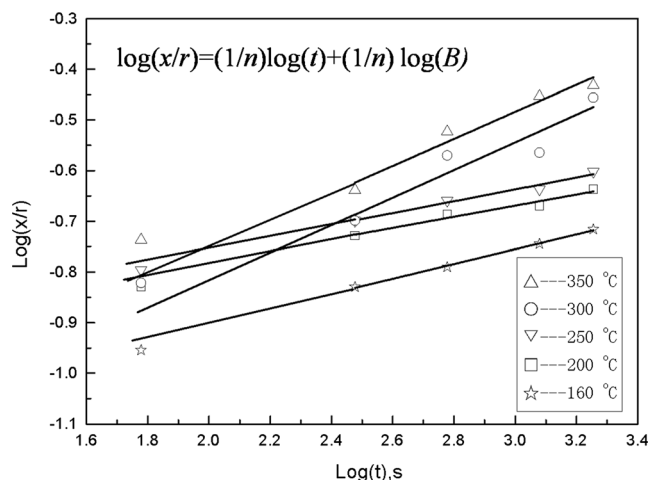
Fig. 4 Neck growth kinetics during sintering process of Ag nanoparticles at different temperatures
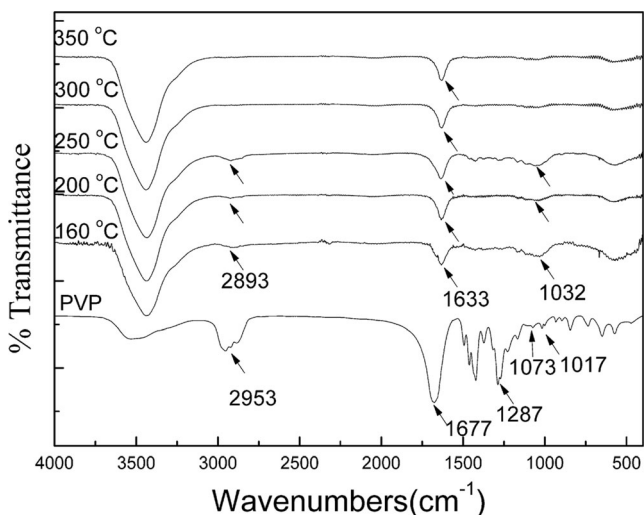
Fig. 5 FTIR spectrums of PVP and Ag nanoparticle paste after being sintered at different temperatures

is below 250 °C, the PVP was still coated on the Ag particles and surface diffusion was the dominant diffusion mechanism during the sintering of Ag nanoparticle paste. When the temperature increases above to 300 and 350 °C, the PVP coated on the Ag particles is destroyed and the main sintering mechanism changes to volume diffusion predominant. This indicates that the sintering mechanisms may be related with the decomposition of organic components in the Ag nanoparticle paste with temperature increasing. Further research is needed to determine the effects of organic components and content on the sintering behaviors and bondability of Ag nanoparticle paste.

3.3 Strength of joints bonded using Ag nanoparticles

The strength is one of the important properties of the joint, and it is interesting to study the strength model bonded using Ag nanoparticle paste. Although some empirical and theoretical relationships have been proposed to describe the dependence of mechanical properties on the microstructure of sintered materials, few reports have been published about the joint strength evolution about the sintering bonding technology using Ag nanoparticle paste [36, 37]. In this work, the joints bonded with Ag nanoparticles were predominantly fractured in the sintered Ag layers [22]. This indicates that the poor area of joint is in the sintered Ag paste instead of the interface between Ag paste and Ag-coated substrate. The joint strength is closely related to the microstructure of the sintered Ag nanoparticle paste. It is found that obvious fracture of interparticle bonds corresponds to the high joint strength. It is reasonable to assume that the strength of the joint with Ag nanoparticle paste arises from the sintered bond formed between contacting Ag particles.

In order to relate joint strength to microstructure, we base our analysis on the classical sphere-to-sphere model as shown

in Fig. 3. In this model, the bond between contacting particles dictates strength. It is assumed that the joint strength depends on the inherent material strength τ_o and the percent of interface area involved in the bond. The percent of interface area involved in the bond should be proportional to the ratio of effective bond area between the adjacent particles.

As shown in the sintering model, the interface area between the two contacting particles is calculated as follows:

$$s = \pi x^2 \tag{5}$$

where s is the interface area between the contacting particles and x is the neck radius. The area of the sphere section of the initial particle is given as follows:

$$S = \pi r^2 \tag{6}$$

where S is the sphere section area of the contacted particle and r is the initial radius. Therefore, the ratio of effective bond area (R) in each particle is expressed as follows:

$$R = s/S = \left(\pi x^2\right)/\left(\pi r^2\right)(x/r)^2 \tag{7}$$

According to the transverse rupture strength model developed by German [37], the joint strength is also related to the fractional density V_s, effective number of bonds Nc/π, and the stress concentration factor K. Therefore, it is suggested that the shear strength using Ag nanoparticles is expressed as follows:

$$\tau = V_s(N_c/K\pi)\tau_o R = V_s(N_c/K\pi)\tau_o(x/r)^2 \tag{8}$$

where τ is the measured shear strength and τ_o is bulk material strength. V_s and N_c are the fractional density and coordination number, respectively. R is the ratio of effective bond area in each particle. K is the stress concentration factor, and (x/r) is the interparticle neck size ratio.

To validate the relationship of joint strength and ratio of effective bond area in each particle, we perform shear test on the joints and plot the shear strength of the joints against the corresponding interparticle neck size ratio $(x/r)^2$. The neck size of sintered particles was measured from the fracture surfaces as shown in Fig. 3c. X and D were the diameter of the neck circular and diameter of the particle, respectively, which could be detected from SEM images of fracture surfaces. As shown in Fig. 6, the radius of the neck between the Ag particles is less than a value of ~0.4–0.5 of the particle radius. This indicates that it is reasonable to assume that the initial stage sintering of Ag nanoparticle occurs. When the bonding temperature is in the range of 200–350 °C, there is an approximate linear relation between the shear strength and square of neck size ratio $(x/r)^2$. This result confirms that the
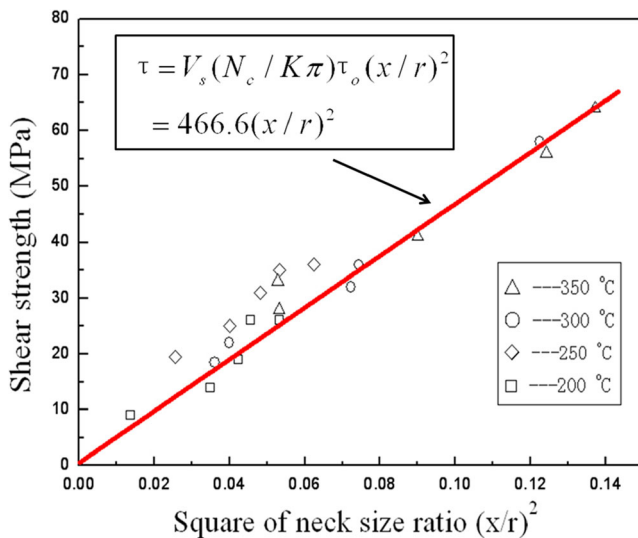
Fig. 6 The relationship between the square of neck size ratio $(x/r)^2$ and the joint strength based on the sphere-to-sphere model

shear strength of the joint is proportional to the ratio of effective bond area in each particle. In Fig. 6, the slope of the fitting straight line by the least square method is 466.6. The relation between joint strength and square of neck size ratio is expressed as follows:

$$\Gamma = 466.6(x/r)^2 \qquad (9)$$

According to this sintering model, it is clear that the inter-particle bond between the sintered adjacent particles is one of the primary sources of strength. It is reasonable to deduce that strength of the joints can be improved by increasing the sintering degree of Ag nanoparticles. Based on this, it is known that the strength of the joint with Ag nanoparticle paste is generally improved with the increase of sintering temperatures or assistance of bonding pressure, which helps to increase the sintering degree of Ag nanoparticles.

4 Conclusions

In this work, the Ag nanoparticle paste is prepared by the chemical reduction method, and the sintering bonding process using Ag nanoparticle paste is investigated. The classical sphere-to-sphere model is introduced to study the sintering mechanisms of Ag nanoparticles during the bonding process. The surface diffusion seems to be the dominant diffusion mechanism during the low-temperature sintering of Ag nanoparticles (160–250 °C). With the increase of sintering temperatures (300–350 °C), volume diffusion becomes the main sintering mechanism. It is found that the strength of the joints is depended on the sintering degree of Ag nanoparticles. A proportional relationship between the shear strength and square of neck size ratio $(x/r)^2$ is revealed.

References

1. De M, Ghosh PS, Rotello VM (2008) Adv Mater 20:4225
2. Sun Y, Xia Y (2002) Science 298:2176
3. Zhang XY, Hu A, Zhang T, Lei W, Xue XJ, Zhou Y, Duley WW (2011) ACS Nano 5:9082
4. Lu Y, Liu GL, Lee LP (2004) Nano Lett 5:5
5. Jiang H, Moon K, Li Y, Wong CP (2006) Chem Mater 18:2969
6. Zhang R, Lin W, Moon K-s, Wong CP (2010) ACS Appl Mater Inter 2:2637
7. Goldstein AN, Echer CM, Alivisatos AP (1992) Science 256:1425
8. Allen GL, Bayles RA, Gile WW, Jesser WA (1986) Thin Solid Films 144:297
9. Jiang Q, Zhang SH, Li JC (2004) Solid State Commun 130:581
10. Buffat P, Borel JP (1976) Phys Rev A 13:2287
11. Zhang M, Efremov MY, Schiettekatte F, Olson EA, Kwan AT, Lai SL, Wisleder T, Greene JE, Allen LH (2000) Phys Rev B 62:10548
12. Moon KS, Dong H, Maric R, Pothukuchi S, Hunt A, Li Y, Wong CP (2005) J Electron Mater 34:168
13. Lu Y, Huang JY, Wang C, Sun S, Lou J (2010) Nat Nanotechnol 5:218
14. Cui Q, Gao F, Mukherjee S, Gu Z (2009) Small 5:1246
15. Ko SH, Pan H, Grigoropoulos CP, Luscombe CK, Fréchet JMJ, Poulikakos D (2007) Nanotechnology 18:345202
16. Hu A, Guo JY, Alarifi H, Patane G, Zhou Y, Compagnini G, Xu CX (2010) Appl Phys Lett 97:153117
17. Ide E, Angata S, Hirose A, Kobayashi KF (2005) Acta Mater 53:2385
18. Bai JG, Zhang ZZ, Calata JN, Lu GQ (2006) IEEE Trans Compon Pack Technol 29:589
19. Yan J, Zou G, Wu A, Ren J, Hu A, Zhou Y (2012) Scripta Mater 66:582
20. Alarifi H, Hu A, Yavuz M, Zhou Y (2011) J Electron Mater 40:1394
21. Peng P, Hu A, Zhao B, Gerlich AP, Zhou Y (2012) J Mater Sci 47:6801
22. Yan J, Zou G, Wu A, Ren J, Hu A, Zhou Y (2012) J Electron Mater 41:1924
23. Yan J, Zou G, Hu A, Zhou YN (2011) J Mater Chem 21:15981
24. Bakhishev T, Subramanian V (2009) J Electron Mater 38:2720
25. Johnson RW, Evans JL, Jacobsen P, Thompson JR, Christopher M (2004) IEEE Trans Electron Packag Manuf 27:164
26. Morita T, Ide E, Yasuda Y, Hirose A, Kobayashi K (2008) Jpn J Appl Phys 47:6615
27. Wang H, Qiao X, Chen J, Wang X, Ding S (2005) Mater Chem Phys 94:449
28. Kang SJL (2005) Sintering: densification, grain growth and microstructure. Elsevier, Amsterdam
29. Coble RL (1961) J Appl Phys 32:787
30. Rahaman MN (2003) Ceramic processing and sintering, 2nd edn. Marcel Dekker, New York
31. Frenkel J (1945) J Phys 9:385
32. Shaler AJ, Wulff J (1948) Ind Eng Chem 40:838
33. Kuczynski GC (1949) J Metals Trans AIME 185:169
34. Rockland JGR (1967) Acta Mater 15:277
35. Zhang Z, Zhao B, Hu L (1996) J Solid State Chem 121:105
36. Nyce AC, Shafer WM (1972) Int J Powder Metall 8:171
37. German RM (2001) Mater Trans 42:1400